Broadband tunable terahertz polarization converter based on a sinusoidally-slotted graphene metamaterial

JIANFENG ZHU,[1,2] SHUFANG LI,[1,2,*] LI DENG,[1,2] CHEN ZHANG,[1,2] YANG YANG,[3] AND HONGBO ZHU[4]

[1]*Beijing Key Laboratory of Network System Architecture and Convergence, Beijing University of Posts and Telecommunications, Beijing 100876, China*
[2]*Beijing Laboratory of Advanced Information Network, Beijing University of Posts and Telecommunications, Beijing 100876, China*
[3]*School of Electrical and Data Engineering, University of Technology Sydney, Sydney, Australia*
[4]*Jiangsu Key Laboratory of Wireless Communications, Nanjing University of Posts and Telecommunications, Nanjing, China*
bupt_paper@126.com

Abstract: A new wideband sinusoidally-slotted graphene-based cross-polarization converter (CPC) is proposed in this paper. The proposed polarization converter can realize a broadband terahertz polarization conversion from 1.28 to 2.13-THz with a polarization conversion ratio (PCR) of more than 0.85. Taking advantage of the gradient width modulation of the graphene-based unit structure, the continuous plasmon resonances are excited at the edges of the sinusoidal slot. Therefore, the proposed converter can achieve a broadband polarization conversion in a simplified structure. Furthermore, the polarization conversion characteristics of the CPC are insensitive to the incident angle. The PCR remains more than 0.85 with little bandwidth degradation even as the incident angle increases to as high as 50°. More importantly, the operating bandwidth and the magnitude of the PCR can be tuned easily by adjusting the chemical potential and the electron scattering times of the graphene. In a way, we believe this kind of graphene-based polarization converter can enrich the polarization conversion community for realizing broadband and tunable polarization conversion.

OCIS codes: (160.3918) Metamaterial; (040.2235) Far infrared or terahertz; (250.5403) Plasmonics.

References and links

1. M. Born and E. Wolf, Principles of Optics. Cambridge, U.K.: Cambridge Univ. Press, (1999).
2. Y. Ye and S. He, "90° polarization rotator using a bilayered chiral metamaterial with giant optical activity," Appl. Phys. Lett. **96**(20), 203501 (2010).
3. K. Song, Y. Liu, C. Luo, and X. Zhao, "High-efficiency broadband and multiband cross-polarization conversion using chiral metamaterial," J. Phys. D Appl. Phys. **47**(50), 505104 (2014).
4. J. H. Shi, X. C. Liu, S. W. Yu, T. T. Lv, Z. Zhu, H. F. Ma, and T. J. Cui, "Dual-band asymmetric transmission of linear polarization in bilayered chiral metamaterial," Appl. Phys. Lett. **102**(19), 191905 (2013).
5. H. Chen, J. F. Wang, H. Ma, S. B. Qu, Z. Xu, A. Zhang, M. Yan, and Y. Li, "Ultra-wideband polarization conversion metasurfaces based on multiple plasmon resonances," J. Appl. Phys. **115**(15), 154504 (2014).
6. H. L. Zhu, S. W. Cheung, K. L. Chung, and T. I. Yuk, "Linear-to-circular polarization conversion using metasurface," IEEE Trans. Antenn. Propag. **61**(9), 4615–4623 (2013).
7. H. F. Ma, G. Z. W. G. S. Kong, and T. J. Cui, "Broadband circular and linear polarization conversions realized by thin briefringent reflective metasurfaces," Opt. Mater. Express **4**(8), 1717–1724 (2014).
8. Y. F. Li, J. Q. Zhang, S. B. Qu, J. F. Wang, L. Zheng, Y. Q. Pang, Z. Xu, and A. X. Zhang, "Achieving wide-band linear-to-circular polarization conversion using ultra-thin bilayered metasurfaces," J. Appl. Phys. **117**(4), 044501 (2015).
9. L. Wu, Z. Y. Yang, Y. Z. Cheng, M. Zhao, R. Z. Gong, Y. Zheng, J. A. Duan, and X. H. Yuan, "Circular polarization converters based on bi-layered asymmetrical split ring metamaterials," Appl. Phys., A Mater. Sci. Process. **116**(2), 643–648 (2014).
10. L. Wu, Z. Y. Yang, Y. Z. Cheng, M. Zhao, R. Z. Gong, Y. Zheng, J. A. Duan, and X. H. Yuan, "Giant asymmetric transmission of circular pol arization in layer-by-layer chiral metamaterials," Appl. Phys. Lett. **103**(2), 021903 (2013).

11. J. K. Gansel, M. Latzel, A. Frölich, J. Kaschke, M. Thiel, and M. Wegener, "Tapered gold-helix metamaterials as improved circular polarizers," Appl. Phys. Lett. **100**(10), 101109 (2012).
12. Q.-Y. Wen, H.-W. Zhang, Q.-H. Yang, Z. Chen, Y. Long, Y.-L. Jing, Y. Lin, and P.-X. Zhang, "A tunable hybrid metamaterial absorber based on vanadium oxide films," J. Phys. D Appl. Phys. **45**(23), 235106 (2012).
13. D. Wang, L. Zhang, Y. Gu, M. Q. Mehmood, Y. Gong, A. Srivastava, L. Jian, T. Venkatesan, C. W. Qiu, and M. Hong, "Switchable ultrathin quarter-wave plate in terahertz using active phase-change metasurface," Sci. Rep. **5**(1), 15020 (2015).
14. X. Zheng, Z. Xiao, and X. Ling, "A Tunable Hybrid Metamaterial Reflective Polarization Converter Based on Vanadium Oxide Film," Plasmonics **13**(1), 287–291 (2018).
15. Z. Xiao, H. Zou, X. Zheng, X. Ling, and L. Wang, "A tunable reflective polarization converter based on hybrid metamaterial, " Opt. Quant. Electron. 49, 12 (2017).
16. D. Shrekenhamer, W.-C. Chen, and W. J. Padilla, "Liquid crystal tunable metamaterial absorber," Phys. Rev. Lett. **110**(17), 177403 (2013).
17. N.-H. Shen, M. Kafesaki, T. Koschny, L. Zhang, E. N. Economou, and C. M. Soukoulis, "Broadband blueshift tunable metamaterials and dual-band switches," Phys. Rev. B **79**(16), 161102 (2009).
18. J. Zhu, Y. Yang, and S. Li, "A photo-excited broadband to dual-band tunable terahertz prefect metamaterial polarization converter," Opt. Commun. **413**, 336–340 (2018).
19. Y. Cheng, R. Gong, and J. Zhao, "A photoexcited switchable perfect metamaterial absorber/reflector with polarization-independent and wide-angle for terahertz waves," Opt. Mater. **62**, 28–33 (2016).
20. J. Zhao, Y. Cheng, and Z. Cheng, "Design of a Photo-Excited Switchable Broadband Reflective Linear Polarization Conversion Metasurface for Terahertz Waves," IEEE Photonics J. **10**(1), 1–10 (2018).
21. S. Zhang, J. Zhou, Y. S. Park, J. Rho, R. Singh, S. Nam, A. K. Azad, H. T. Chen, X. Yin, A. J. Taylor, and X. Zhang, "Photoinduced handedness switching in terahertz chiral metamolecules," Nat. Commun. **3**(1), 942–948 (2012).
22. A. K. Geim and K. S. Novoselov, "The rise of graphene," Nat. Mater. **6**(3), 183–191 (2007).
23. A. K. Geim, "Graphene: Status and prospects," Science **324**(5934), 1530–1534 (2009).
24. L. Ye, Y. Chen, G. Cai, N. Liu, J. Zhu, Z. Song, and Q. H. Liu, "Broadband absorber with periodically sinusoidally-patterned graphene layer in terahertz range," Opt. Express **25**(10), 11223–11232 (2017).
25. R. Alaee, M. Farhat, C. Rockstuhl, and F. Lederer, "A perfect absorber made of a graphene micro-ribbon metamaterial," Opt. Express **20**(27), 28017–28024 (2012).
26. B. Z. Xu, C. Q. Gu, Z. Li, and Z. Y. Niu, "A novel structure for tunable terahertz absorber based on graphene," Opt. Express **21**(20), 23803–23811 (2013).
27. Z. Su, J. Yin, and X. Zhao, "Terahertz dual-band metamaterial absorber based on graphene/MgF2 multilayer structures," Opt. Express **23**(2), 1679–1690 (2015).
28. Y. Zhang, Y. Feng, B. Zhu, J. Zhao, and T. Jiang, "Graphene based tunable metamaterial absorber and polarization modulation in terahertz frequency," Opt. Express **22**(19), 22743–22752 (2014).
29. A. Andryieuski and A. V. Lavrinenko, "Graphene metamaterials based tunable terahertz absorber: effective surface conductivity approach," Opt. Express **21**(7), 9144–9155 (2013).
30. H. Xiong, Y. B. Wu, J. Dong, M. C. Tang, Y. N. Jiang, and X. P. Zeng, "Ultra-thin and broadband tunable metamaterial graphene absorber," Opt. Express **26**(2), 1681–1688 (2018).
31. H. Cheng, S. Chen, P. Yu, J. Li, B. Xie, Z. Li, and J. Tian, "Dynamically tunable broadband mid-infrared cross polarization converter based on graphene metamaterial," Appl. Phys. Lett. **103**(22), 223102 (2013).
32. H. Cheng, S. Chen, P. Yu, J. Li, L. Deng, and J. Tian, "Mid-infrared tunable optical polarization converter composed of asymmetric graphene nanocrosses," Opt. Lett. **38**(9), 1567–1569 (2013).
33. Y. Huang, Z. Yao, F. Hu, C. Liu, L. Yu, Y. Jin, and X. Xu, "Tunable circular polarization conversion and asymmetric transission pf planar chiral graphene-metamaterial in terahertz region," Carbon **119**, 305–313 (2017).
34. S. Luo, B. Li, A. Yu, J. Gao, X. Wang, and D. Zuo, "Broadband tunable terahertz polarization converter based on graphene metamaterial," Opt. Commun. **413**, 184–189 (2018).
35. Y. V. Bludov, M. I. Vasilevskiy, and N. M. R. Peres, "Tunable graphene-based polarizer," J. Appl. Phys. **112**(8), 084320 (2012).
36. X. Yu, X. Gao, W. Qiao, L. Wen, and W. Yang, "Broadband tunable polarization converter realized by graphene-based metamaterial," IEEE Photonics Technol. Lett. **28**(21), 2399–2402 (2016).
37. C. Yang, Y. Luo, J. Guo, Y. Pu, D. He, Y. Jiang, J. Xu, and Z. Liu, "Wideband tunable mid-infrared cross polarization converter using rectangle-shape perforated graphene," Opt. Express **24**(15), 16913–16922 (2016).
38. J. Ding, B. Arigong, H. Ren, M. Zhou, J. Shao, Y. Lin, and H. Zhang, "Efficient multiband and broadband cross polarization converters based on slotted L-shaped nanoantennas," Opt. Express **22**(23), 29143–29151 (2014).
39. J. Ding, B. Arigong, H. Ren, J. Shao, M. Zhou, Y. Lin, and H. Zhang, "Mid-infrared tunable dual-frequency cross polarization converters using graphene-based L-shaped nanoslot array," Plasmonics **10**(2), 351–356 (2015).
40. Z. Li, K. Yao, F. Xia, S. Shen, J. Tian, and Y. Liu, "Graphene plasmonic metasurfaces to steer infrared light," Sci. Rep. **5**(1), 12423 (2015).
41. M. Chen, L. Chang, X. Gao, H. Chen, C. Wang, X. Xiao, and D. Zhao, "Wideband Tunable Cross Polarization Converter Based on a Graphene Metasurface With a Hollow-Carved "H" Array," IEEE Photonics J. **9**(5), 1–11 (2017).

42. X. Gao, W. Yang, W. Cao, M. Chen, Y. Jiang, X. Yu, and H. Li, "Bandwidth broadening of a graphene-based circular polarization converter by phase compensation," Opt. Express **25**(20), 23945–23954 (2017).
43. N. M. R. Peres, A. Ferreira, Y. V. Bludov, and M. I. Vasilevskiy, "Light scattering by a medium with a spatially modulated optical conductivity: the case of graphene," J. Phys. Condens. Matter **24**(24), 245303 (2012).
44. G. W. Hanson, "Dyadic Green's functions and guided surface waves for a surface conductivity model of graphene," J. Appl. Phys. **103**(6), 064302 (2008).
45. L. Wang, J. Zhang, N. Liu, Y. Wang, P. A. Hu, and Z. Wang, "Fast patterned graphene ribbons via soft lithography," Procedia CIRP **42**, 428–432 (2016).
46. G. Jo, M. Choe, C. Y. Cho, J. H. Kim, W. Park, S. Lee, W. K. Hong, T. W. Kim, S. J. Park, B. H. Hong, Y. H. Kahng, and T. Lee, "Large-scale patterned multi-layer graphene films as transparent conducting electrodes for GaN light-emitting diodes," Nanotechnology **21**(17), 175201 (2010).
47. E. Carrasco, M. Tamagnone, and C. J. Perruisseau, "Tunable graphene reflective cells for THz reflectarrays and generalized law of reflection," Appl. Phys. Lett. **102**(10), 104103 (2013).

1. Introduction

As one of the most fundamental properties of manipulating electromagnetic (EM) waves, polarization manipulation has received considerable attention from various aspects. Conventional approaches to realize polarization manipulation includes the use of photo-elastic modulators and optical gratings [1]. Although these methods can manipulate the polarization at will, they usually require large equipment and a long propagation distance to achieve the phase accumulation. To ease the burdens mentioned above, metamaterial, an artificial subwavelength composite material with unique electromagnetic (EM) responses, has been widely used to manipulate the polarization states. In fact, metamaterials have been increasingly associated with the polarization since it is developed due to its exceptional properties. To date, plenty of metamaterial-based linear-to-linear [2–5], linear-to-circular [6–8] and circular-to-circular [9–11] polarization manipulation devices have been proposed. For example, using chiral metasurface combining the Fabry-Perot cavity resonance [3–5], broadband and multiband asymmetry transmission were realized with high transmission efficiency. Taking advantages of the phase-response differences of the orthogonal I-shaped birefringent reflective metasurface, linear to linear, linear-to-circular reflection polarization conversion with wide conversion band was realized in [7]. Nevertheless, though these designs exhibit high polarization conversion efficiency, the polarization conversion band of them cannot be tuned once the patterned structures are fixed, which hinders them toward more widespread applications. On the other hand, tunable composite metamaterials are capable of dynamically manipulating the terahertz (THz) waves with great flexibility by using external stimulus such as thermal [12–15], electric bias [16] and photo-excitation [17–21], which open a bright perspective to design versatile devices. For example, by hybridizing a phase change material, vanadium dioxide (VO2), with a metasurface, switchable ultrathin terahertz quarter-wave plate was realized with extremely low-profile [13]. With photo-excitation, the handedness switching in chiral metamolecules was achieved, which allows electromagnetic control of the polarization of light and it will find important applications in the manipulation of terahertz waves [21]. As the unprecedented development of the THz science and technology, designing such versatile devices with tunable capability is not only desirable but also inevitable for filling the THz gap.

Graphene, a single two-dimensional plane of carbon atoms arranged in a honeycomb lattice, has been theoretically and experimentally demonstrated to excite and propagate surface plasmons with reasonable loss [22,23]. Due to its unique electrical and optical properties in the terahertz and mid-infrared regimes, many intriguing applications have been proposed, such as the optical devices, plasmon waveguiding, clocking devices and many other optoelectronic applications. Compared with metal plasmonics with restricted flexible permittivity, the most remarkable advantage of the graphene is its capability of dynamically tuning the conductivity through straightforward chemical or electrostatic gatings, which opens the door to many exciting tunable devices, such as tunable absorbers [24–30], and tunable polarization converters [31–40]. For example, Cheng et al. proposed a dynamically tunable broadband cross polarization converter (CPC) made of L-shaped graphene sheets,

which transformed linear light into cross polarization light for a single band in the mid-infrared regions [31]. Nanocross has also been used in to efficiently convert the polarization states [32], [34]. Other structures, such as Hollow-Carved "H" Array [41], butterfly-shaped holes [42], have also been demonstrated to be suitable to achieve high polarization conversion efficiency. Nevertheless, most of these polarization devices work at the mid-infrared range with relatively narrow bandwidth. With so many fascinating and exciting features of the graphene, designing the dynamically tunable THz polarization converter with wideband and high efficiency based on the graphene remains an ongoing interest among the researchers to manipulate the THz waves.

In this paper, a new wideband net-shaped sinusoidally-patterned graphene-based CPC is proposed. The polarization converter can realize a broadband terahertz polarization conversion from 1.28 to 2.13-THz with PCR more than 0.85. Based on the unique characteristics of the graphene, the operating bandwidth and magnitude of the PCR can be tuned by adjusting the chemical potential and the electron scattering times. Taking advantages of the gradient width modulation of the graphene-based unit structure, the continuous plasmon resonances are excited at the edges of the slot, and thus the proposed converter can achieve a broadband polarization conversion in a much simpler structure compared with other conventional broadband converter using multi-layered or multi-resonator structures. More importantly, as one of the most exciting features, the polarization conversion characteristic of the CPC is insensitive to the incident angle. The PCR remains more than 0.85 even the incident angle increases to as high as 50°. With these good features, we believe this kind of graphene-based polarization converter can be potentially used in the THz applications.
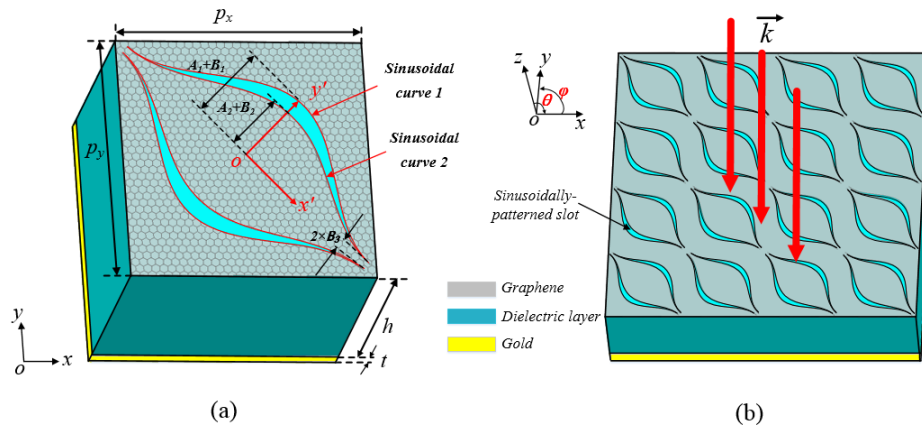

Fig. 1. (a) Unit cell of the proposed CPC. (b) Configurations of the proposed polarization converter, where θ is the incident angle, φ is azimuth angle.

2. The proposed structure and simulation

The proposed graphene-based broadband THz polarization converter is a sandwich structure with graphene sheet on the top, the ground plane on the bottom and a dielectric layer as the spacer, as shown in Fig. 1. The proposed converter was simulated and optimized by using the Finite Element Method (FEM). The periodical boundary conditions are applied in the x- and y-directions, whereas Floquet port is adopted in the z-direction. Since the strain field should have the same period of the patterned substrate, the optical conductivity of graphene will be spatially modulated with the period of the patterned substrate due to strain [43]. In the FEM-based simulation, the periodic spatial modulation of the graphene conductivity is taken into account by making use of the Floquet-Bloch theorem. In the design, the ground metallic continuous film was made of lossy gold with a conductivity of $\sigma = 4.56 \times 10^7$ S/m and a thickness of 0.4 μm. The dielectric layer is the quartz substrate with a thickness of 25 μm (h),

the relative permittivity is 3.75 and the loss tangent is 0.0184. The sinusoidally patterned slot on the graphene layer is composed of two sinusoidal curves, namely. sinusoidal curve 1 and curve 2, as shown in Fig. 1(a). Under the x'oy' coordinate system, which is 45° clock-wise rotated with respect to the xoy coordinate system, the two curves can be expressed as:

$$sinusoidal\ curve\,1: y' = A_1\cos(px') + B_1 \tag{1}$$

$$sinusoidal\ curve\,2: y' = A_2\cos(px') + B_2 \tag{2}$$

where the optimized parameters of the proposed converter are as follows: p_x = 16 μm, p_y = 16 μm, h = 25 μm, t = 0.4 μm, A_1 = 2.54 μm, A_2 = 2.0 μm, B_1 = 2.84 μm, B_2 = 2.3 μm, B_3 = 0.3 μm and p = 0.3. The lattice period is 16 μm and the length of the slit is about 23.6 um, corresponding to about 0.09 and 0.13 wavelength at 1.6 THz, respectively.

The conductivity of graphene is characterized by the sum of intra-band conductivity and inter-band conductivity. In the low THz operation frequency and room temperature, intra-band conductivity mainly determines the conductivity of the graphene and the inter-band conductivity can be neglected. Considering its one-atom thickness, the surface conductivity σ of graphene in the intraband can be calculated by the Drude model [44]:

$$\sigma_{intra}(\omega,\mu_c,\Gamma,T) = -j\frac{e^2 k_B T}{\pi\hbar^2(\omega - j2\Gamma)}(\frac{\mu_c}{k_B T} + 2\ln(e^{-\frac{\mu_c}{k_B T}} + 1)). \tag{3}$$

where e is the electron charge, k_B is the Boltzmann's constant, $\hbar$ is the reduced Plank's constant. T is temperature, τ is the relaxation time, ω is the radian frequency, and μ_c is chemical potential. In the design, the room temperature is set to 300 K, the typical value of relaxation time of graphene is τ = 1 ps, and the chemical potential μ_c is set to 0.4 eV. It is also worth to note that the sinusoidally patterned slot on graphene can be obtained through optical or electron beam lithography [45], [46].
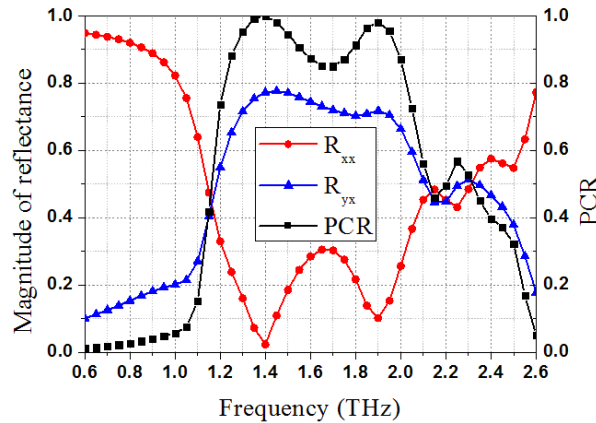

Fig. 2. The magnitudes of the reflectance and the PCR of the proposed CPC.

3. Theoretical analyses and results discussion

The reflection coefficient of the CPC is characterized by its 2 × 2 scattering matrices as the following:

$$R = \begin{pmatrix} R_{xx} & R_{xy} \\ R_{yx} & R_{yy} \end{pmatrix} \tag{4}$$

where R_{xx}, R_{xy}, R_{yx}, R_{yy} represent the complex reflection ratio of the x-to-x, y-to-x, x-to-y and y-to-y polarizations, respectively. Due to the symmetry of the CPC, $R_{xx} = R_{yy}$ and $R_{xy} = R_{yx}$. Therefore, only R_{xx} and R_{yx} are discussed by considering x-polarized incident waves for brevity without loss of generality. To evaluate the polarization conversion performance, the polarization conversion ratio is defined as:

$$PCR = \left(\frac{|R_{yx}|^2}{|R_{xx}|^2 + |R_{yx}|^2} \right) \tag{5}$$

Figure 2 shows the R_{xx}, R_{yx} and the PCR of the proposed CPC, where the Fermi energy of graphene and the electron scattering time are 0.4 eV and 1 ps, respectively. The PCR is clearly observed to be above 85% from 1.3 THz to 2.1 THz with full-width-at-half-maximum (FWHM) reaching 47%. Figure 3 depicts the electric field distributions at the surface of the graphene sheet at 0.6, 1.45 and 2.0-THz, respectively. The electric field distributions are in accordance with the PCR spectrum. For instance, at 0.6 THz that out of the polarization conversion band, the electric field almost vanished, indicating that no localized plasmon resonance is excited. Whereas in the 1.45 and 2.0-THz with high PCR shown in the Fig. 2, the electric field distributions are concentrated at the edges of the sinusoidal slots, where the localized surface plasmon resonances are excited.
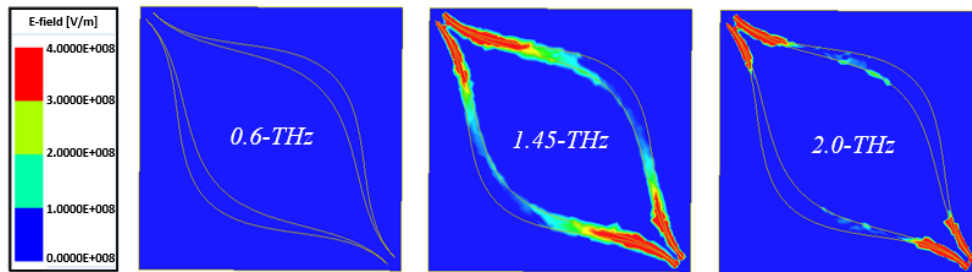

Fig. 3. The magnitude of electric field distributions at 0.6, 1.45 and 2.0-THz.

To better reveal the physical mechanism of the proposed graphene-based CPC. The surface current distributions and the induced magnetic field distributions at the top graphene sheet and the bottom ground, for the two resonant modes at 1.45 THz and 2.0 THz are shown in Fig. 4 when the electric field of the incident waves are parallel to the x-axis. It can be seen from Fig. 4(a_3) that, at 1.45 THz, the induced magnetic field targets at the lower-left direction, which can be decomposed into two orthogonal magnetic vector H_{lx} along the x-direction and H_{ly} along the y-direction. The H_{ly}, perpendicular to the electric field of the x-polarized incident waves, will not generate cross-polarization coupling since the direction of the magnetic fields is the same to that of the incident waves. Whereas the magnetic fields along the x-direction can induce the electric field along the y-direction, consequently leading to the cross-polarization conversion. At the higher localized plasma resonant mode, as shown in Fig. 4(b_3), the magnetic fields are along the upper right direction, and the x-component of the magnetic field can induce the electric field along the y-direction, leading to the cross-polarization conversion. In fact, the CPC is related to two orthogonal eigen modes, namely eigen mode 1 with 45° counterclockwise from the incident waves (x-direction) and eigen mode 2 with 45° clockwise from the incident waves. The polarization is rotated by about 90° because of the combination of the two eigen modes in the reflection states. Figure 5 shows the reflection coefficients and also the phase differences of the two eigen modes. It is observed that the reflection of these two orthogonal eigen modes have a nearly 180° phase difference at two resonant frequencies, which leads to the high cross-polarization efficiency. According to Fig. 5, it is also seen that, from at 1.8-1.9 THz band, the magnitudes of the reflection of the

two eigen modes show a difference of 0.1. The difference of the magnitudes of the reflection results in the PCR in 1.8-1.9 THz band a little bit lower than the neighboring spectrum.
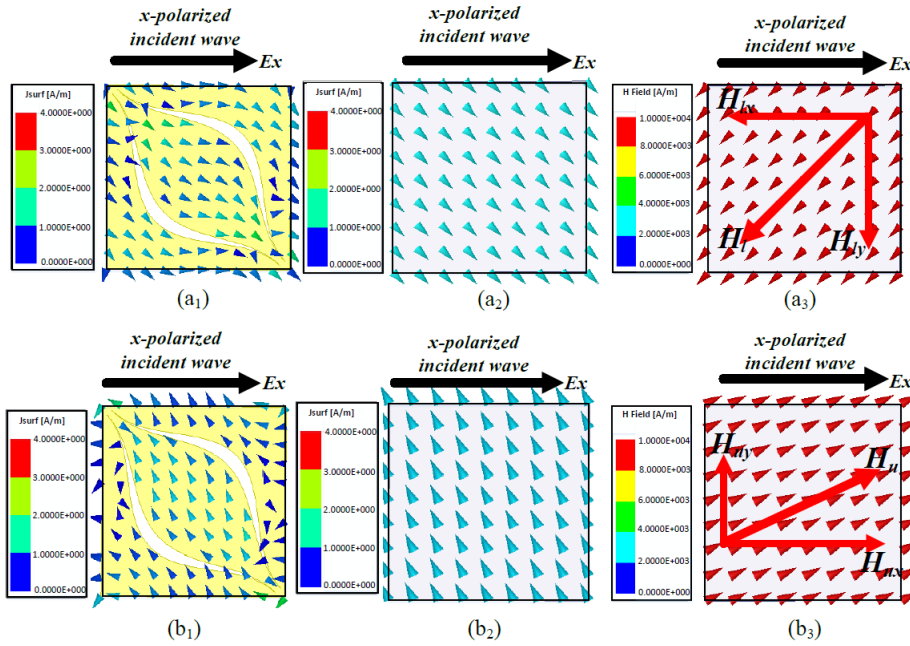

Fig. 4. Surface current distributions at 1.45 THz at the top (a_1), bottom layer (a_2) and the induced magnetic field distributions at the bottom layer (a_3). Surface current distributions at 2.0 THz at the top (b_1), bottom layer (b_2) and the induced magnetic field distributions at the bottom layer (b_3).
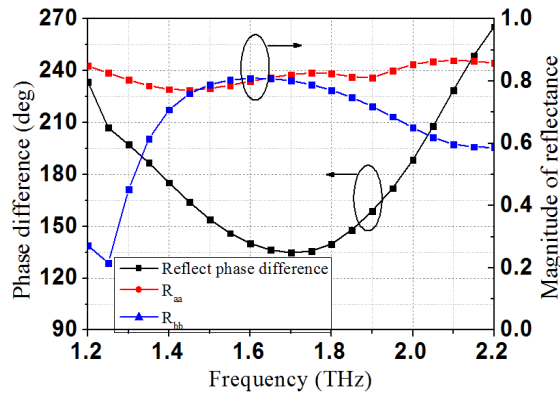

Fig. 5. Simulated results of reflectance for the two orthogonal eigen modes with the incident polarization of 45° (R_{aa}) and −45° (R_{bb}) clockwise from the x-axis direction and the reflected phase difference of them.
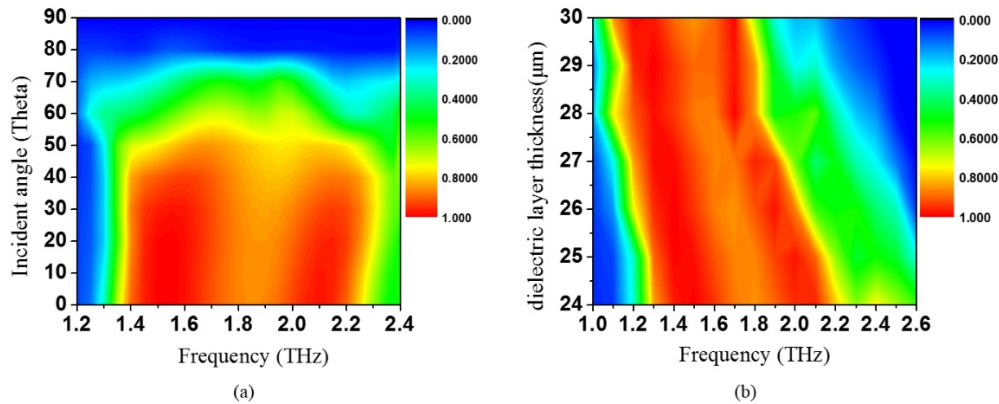
Fig. 6. (a) PCR spectrum of the proposed CPC as a function of the operating frequency and incident angle with μ_c = 0.4 eV and τ = 1 ps. (b) PCR spectrum of the proposed CPC as a function of the operating frequency and thickness of the dielectric layer with μ_c = 0.4 eV and τ = 1 ps.

Since the continuously localized plasmon resonances, which are excited at the edges of the gradient width sinusoidally-patterned slots, contributes to the broadband cross-polarization conversion, the bandwidth of the PCR should less sensitive to the incident angle θ. The PCR spectrum under the incident angle from 0 to 90° is shown in the Fig. 6(a). It is observed that the proposed CPC shows very stable performance over large incident angles. Specifically, the PCR can be kept better than 0.85 with the little bandwidth degradation when the incident angle increases as large as 50°. Compared to some previous designs, the proposed design has the inherent merits of broad bandwidth of polarization conversion and large incident angle insensitivity, which enables the proposed CPC to have more widespread applications such as in terahertz sensing, detecting, and optoelectronic devices. It is also noticed that, when the incident angle further increases to 90°, the large attenuation of the PCR is observed. This is due to the fact that the increased incident angle results in a weakened interaction between the graphene sheet and the electromagnetic waves. Figure. 6(b) depicts the PCR spectrum with different values of the dielectric thickness when the chemical potential u_c is fixed at 0.4 eV. It is observed that the operating bandwidth exhibits red-shifts due to the fact that the thickness of the dielectric layer is related to the phase response characteristics of the proposed graphene CPC.
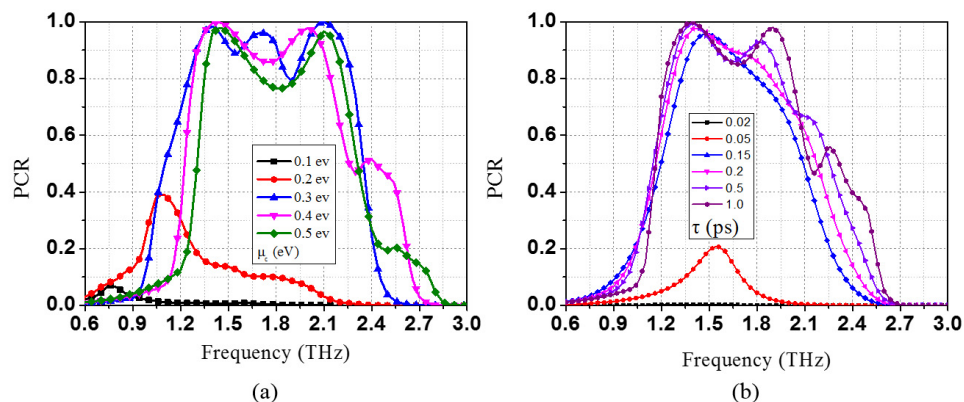

Fig. 7. (a) Simulated PCRs of the proposed CPC for different Fermi energies of graphene. (b) Simulated PCRs of the proposed CPC for different electron scattering times of graphene.

Table 1 Comparisons of the proposed polarization converter with other tunable polarization converters

Ref.	Unit structure	PCR peaks	Relative bandwidth (center frequency)	Max Incident angle (degree) (PCR>0.8)	Tuning mechanism	Remarks
[14]	E-shaped hybrid metamaterial	98.9%	61.9% (7.17 THz)	Not given	Temperature control	High PCR, wide bandwidth, fixed band with tunable PCR
[15]	I-shaped resonators	>90%	84.5% (3.6 THz)	30	Temperature control	High PCR, wide bandwidth, fixed band with tunable PCR
[20]	Split ring resonator	99%	83% (1.1 THz)	Not given	Photo-excited	High PCR, wide bandwidth, fixed band with tunable PCR
[36]	I-shaped resonators	>90%	81% (0.67THz)	40	Tunable graphene	High PCR, wide bandwidth, large incident angle
[37]	rectangle-shape resonator	>90%	5% (46.8 THz)	40	Tunable graphene	High PCR, medium bandwidth, large incident angle
[38]	L-shaped resonator	>90%	≈3%(31.5 THz & 41.3 THz)	Not given	Tunable graphene	High PCR, dual frequency band tunable
[39]	Slotted nanoarray	>95%	38.5% (78 THz)	45	Tunable graphene	High PCR, wide bandwidth, large incident angle
This work	sinusoidally-patterned graphene	97.2%	47% (1.7 THz)	>50	Tunable graphene	High PCR, wide bandwidth, large incident angle

Furthermore, the electrostatic tunability of the proposed graphene CPC is investigated. Figure 7(a) plots the PCRs of different Fermi energy levels under the normal incidence. It can be seen the operating frequency band shows a blue shift when the Fermi energy increases from 0.1 eV to 0.5 eV. The PCR values increase rapidly to its maximum when the Fermi energy increases to above 0.3 eV, which is due to the fact that the higher Fermi energy not only leads to the decrease of the inherent loss of the graphene but also results in a stronger plasma resonance. Then, the reflected orthogonal components achieve nearly 180° phase difference in two reflected orthogonal components and thus the perfect polarization conversion. Figure 7(b) shows the PCR curves for different electron scattering times of the graphene under normal incidence with Fermi energy is fixed at 0.4 eV. There is almost no polarization conversion when the electron scattering time τ is 0.02 ps. When the τ is increased to more than 0.15, high polarization conversion efficiency is achieved with broad bandwidth. This is because by increasing the values of τ, the plasmonic oscillation becomes stronger, leading to a plasmonic conversion. The proposed CPC with flexible tunability and simple structure may be used as a tunable broadband modulator at terahertz frequencies. For practical experiment, we may design the graphene-based polarization converter that consists of five layers including a graphene layer, an insulator layer of Al_2O_3, a polycrystalline silicon layer, a dielectric layer, and the ground. The DC voltage is applied between polycrystalline silicon layer and the graphene using Al_2O_3 (Alumina, $\varepsilon_r = 8.9$ and $\tan\delta = 0.01$) as spacer, similar to the fabrication design in [47].

Table 1 compares the key characteristics of the proposed polarization converter with other state-of-the-art works. Although the tunable polarization converters realized by using thermal

[14], [15] and photo-excitation [20] can achieve high PCR over a wide bandwidth, only the magnitude of the PCR can be tuned whereas the frequency band is fixed. Compared with other graphene-based tunable polarization converters [37], [38], the proposed one exhibits wider bandwidth and higher PCR. Although new designs of polarization converters, such as using I-shaped resonators [36] and slotted nanoarrays [39], achieve high PCR over a wide bandwidth, their PCRs decrease fast when the incident angle increases greater than 30°. Whereas the proposed polarization converter not only achieves high PCR over a wide bandwidth but also maintains the efficient and stable polarization conversion capability over wide incident angles due to the continuous localized plasmon resonances excited. With the good features, the proposed polarization converter can be potentially used in the THz applications.

Conclusion

In summary, a new wideband net-shaped sinusoidally-patterned graphene-based CPC is proposed. The polarization converter can realize a broadband terahertz polarization conversion from 1.28 to 2.13-THz with PCR more than 0.85. The operating bandwidth and magnitude of the PCR can be tuned easily by adjusting the chemical potential and the electron scattering times. Moreover, the polarization conversion feature is insensitive to the incident angle due to the continuous localized plasmon resonances excited. The PCR remains more than 0.85 even the incident angles increases as high as 50°. The wideband, high PCR and incident angle insensitivity demonstrate the proposed polarization converter can be used in the THz applications.

Funding